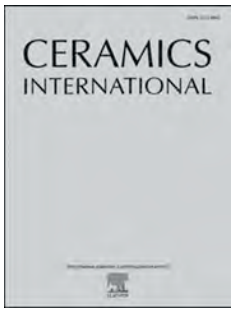

Correlations between structure and microwave dielectric properties of Co doped $MgMoO_4$ ceramics

Wenjie Bian, Xiaochi Lu, Yan Wang, Haikui Zhu, Tao Chen, Shiwo Ta, Qitu Zhang

PII: S0272-8842(20)31475-9

DOI: https://doi.org/10.1016/j.ceramint.2020.05.187

Reference: CERI 25288

To appear in: *Ceramics International*

Received Date: 26 March 2020

Revised Date: 5 May 2020

Accepted Date: 18 May 2020

Please cite this article as: W. Bian, X. Lu, Y. Wang, H. Zhu, T. Chen, S. Ta, Q. Zhang, Correlations between structure and microwave dielectric properties of Co doped $MgMoO_4$ ceramics, *Ceramics International* (2020), doi: https://doi.org/10.1016/j.ceramint.2020.05.187.

Correlations between structure and microwave dielectric properties of Co doped $MgMoO_4$ ceramics

Wenjie Bian[1,2], Xiaochi Lu[1,2], Yan Wang[1,2], Haikui Zhu[1,2,*], Tao Chen[3], Shiwo Ta [3], Qitu Zhang[1,2,*]

Abstract

$Mg_{1-x}Co_xMoO_4$ (x = 0.01–0.15) ceramics were prepared by traditional solid-state methods. The phase composition, crystalline structure, micromorphology, and microwave dielectric properties of $Mg_{1-x}Co_xMoO_4$ ceramics were comprehensively studied. $Mg_{1-x}Co_xMoO_4$ ceramics present monoclinic wolframite structures from x = 0.01 to x = 0.15 with Co occupying the Mg-site. With the addition of Co^{2+}, ε_r of $Mg_{1-x}Co_xMoO_4$ ceramics increase. $Q\times f$ is maximal at 5 mol% Co^{2+} content. The $Mg_{0.95}Co_{0.05}MoO_4$ ceramic exhibits an optimal microwave dielectric property: ε_r = 7, $Q\times f$ = 59247 GHz, τ_f = -68 ppm/°C. The $Q\times f$ values increase by 20 % compared with the pure $MgMoO_4$ ceramics (~ 49149 GHz). Doping Co^{2+} effectively promotes the densification of ceramics and increases ε_r and $Q\times f$. However, when the Co content exceeds 5 mol%, the decreased packing fraction and disorder distribution of ions contribute to the increase in dielectric losses. The correlations between Co^{2+} substitution and wolframite structure have been discussed by Raman spectroscopy, FT-IR spectroscopy and Rietveld refinement.

Key words: Disordered distribution; MoO_4 tetrahedron; Microwave dielectric properties

[1] College of Materials Science and Engineering, Nanjing Tech University, Nanjing 210009, China

[2] Jiangsu Collaborative Innovation Center for Advanced Inorganic Function Composites, Nanjing 210009, China

[3] State Key Laboratory of Advanced Materials and Electronic Components, Zhaoqing 526060, China.

[*] Corresponding Author: Qitu Zhang, E-mail: ngdzqt@163.com
Haikui Zhu, E-mail: zhk@njtech.edu.cn

1 Introduction

For the past few years, the development of wireless communication systems, including filters, resonators, antennas and mobile communication, has set off an upsurge of researching microwave dielectric ceramics with high-frequency applications and low dielectric loss[1-6]. The integration and miniaturization of microwave devices require the maturity of LTCC technology [7]. Microwave dielectric ceramic with low sintering temperature (< 1000 °C) must be developed.

$AMoO_4$ ceramics are potential materials for LTCC technology applications because of their low sintering temperature and appropriate properties. $AMoO_4$ ceramics present two different structures according to the size of A-site ions. The first type is scheelite with the A-site ionic radius over 1.0 Å, such as Ca^{2+}, Sr^{2+}, Ba^{2+} [8-10]. When the A-site ionic radius is less than 1.0 Å, such as Co^{2+}, Mg^{2+}, and Zn^{2+}, the compounds present a wolframite structure[8, 11]. Scheelite $AMoO_4$ ceramics have low dielectric loss, but the high sintering temperature (~ 1100 °C) limits its application in LTCC technology [12]. However, wolframite $AMoO_4$ ceramics with lower sintering temperature (< 1000 °C) show superior microwave dielectric properties [11, 13]. For example, $ZnMoO_4$ ceramics show optimal microwave dielectric properties: ε_r = 9.7, $Q\times f$ = 49990 GHz, and τ_f = -87 ppm/°C when they are sintered at 800 °C[13].

$MgMoO_4$ ceramic is a type of typical wolframite ceramics. In our previous work, $MgMoO_4$ ceramics presented an optimal microwave dielectric property with ε_r = 7, $Q\times f$ = 49149 GHz, and τ_f = -70 ppm/°C at 950 °C. From the crystallography perspective, ionic substitution can tune the microwave dielectric properties by forming solid solutions. However, studies on the correlations between ionic substitution on the wolframite structure and microwave dielectric properties are rare. For monoclinic scheelite ceramics, Wang et al. reported[14] that the distribution of $(NaBi)^{2+}$ in the A sites could cause structural changes. They found order–disorder states in the A sites of $(Na_{0.5}Bi_{0.5})MoO_4$ crystals using vibrational spectroscopy. The distortion of AO_8 polyhedron and MoO_4 tetrahedron, which are generated by the disorder arrangement of A-site ions, changes the ionic polarizabilities and microwave dielectric properties. Similarly, wolframite $MgMoO_4$ ceramic has monoclinic structure.

Analogous to scheelite, the disorder arrangement of A-site ions and polyhedral distortion may associate with the microwave dielectric properties of $MgMoO_4$ ceramics.

Microwave dielectric properties are affected by ionic polarization which is generated by lattice vibrations[15]. As previous studies reported, vibrational spectroscopy is effective to characterize the changes of internal structure and mechanism of dielectric characteristics. Dielectric losses include internal loss and extrinsic loss. Internal loss is intrinsic loss, including packing fraction, structural distortion, etc. Extrinsic loss is due to abnormal grains, pores, order–disorder, etc[16]. Raman spectra can characterize the order–disorder transformation of structures[17]. FT-IR spectroscopy is a powerful tool to explain the contributions of internal loss or extrinsic loss on the microwave dielectric properties by studying the behaviors of polar phonon modes [18, 19].

In this work, Co doped $MgMoO_4$ ceramics were selected as the experimental object. The ionic radius of Co^{2+} (0.65 Å, CN = 6) is near to Mg^{2+} (0.72 Å, CN = 6). Hence, an $Mg_{1-x}Co_xMoO_4$ solid solution can be theoretically formed. Meanwhile, $CoMoO_4$ has wolframite structure[20], so Co ions prefer to enter the Mg position to form a solid solution. XRD, Raman, FT-IR, SEM and Rietveld refinement were used to systematically analyse the effect of the Co substitution on the microwave dielectric properties and wolframite structure.

2 Experimental

$Mg_{1-x}Co_xMoO_4$ ceramics were prepared using solid-state methods with CoO, MgO and MoO_3 as the starting materials. The mixtures were milled with agate balls and ethanol for 12 h. The mixtures were calcined at 750 °C for 3 h after drying. Then, the calcined powders were re-milled for 12 h and milled with 7 wt% of PVA as the binder. Finally, the powders were pressed into 13 mm × 6.5 mm cylindrical disks under 100 MPa. The disks were sintered at 900-1000 °C for 3 h in air.

The crystalline phase constituents were identified by X-ray diffraction (RigakuD/Max 2500 type, Japan) with Cu Kα radiation (k = 0.15406 nm with 2 h step 0.02). The Rietveld refinement of XRD data was calculated by the GSAS-EXPGUI

program. The micromorphology was displayed by a scanning electron microscope (SEM, Hitachi SU8010, Japan). An X-ray photoelectron spectrometer (ESCALAB 250Xi, Thermo Fisher, USA) was employed to collect XPS spectra to reveal the Co^{2+} chemical status, and the X-ray source was Al-Kα primary radiation. The structural information was obtained by a Raman spectrometer (HR800, Horiba Labram), which used the 514 nm He-Cd laser with 20 mW laser power as the excitation source, and a NICOLET 5700 FT-IR spectrometer (Thermo, America).

The bulk densities were measured by Archimedes method. The microwave dielectric properties were tested at approximately 14 GHz by a Network Analyzer (Agilent E5071C, Malaysia). τ_f was calculated by formula (1)[21]:

$$\tau_f = \frac{f_1 - f_0}{f_0 \times (T_1 - T_0)} \quad (1)$$

f_1 and f_0 are the resonant frequencies at T_1 (80 °C) and T_0 (20 °C), respectively.

3 Results and Discussion

Fig. 1 displays the XRD patterns of $Mg_{1-x}Co_xMoO_4$ (x = 0.01–0.15) ceramics sintered at 975 °C for 3 h. All diffraction peaks in the XRD patterns can be indexed with monoclinic wolframite $MgMoO_4$ phase (PDF-# 72-2153) at x from 0.01 to 0.15. No phase other than $MgMoO_4$ is detected. Notably, the main diffraction peaks slightly move to higher angles when x increases. The peak shift is attributed to the lattice shrinkage. To prove this prediction, as Fig. 2(a) shows, Rietveld refinements with refined reliability factors were performed. The refined cell parameters of $Mg_{1-x}Co_xMoO_4$ ceramics (Table 1) confirm that the cell volume of ceramics reduces with more Co substitution. This phenomenon is due to the smaller ionic radius of Co^{2+} (r_{Co}^{2+} = 0.65 Å) than Mg^{2+} (r_{Mg}^{2+} = 0.72 Å). The results suggest that Co dopes into Mg sites and forms a solid solution of $Mg_{1-x}Co_xMoO_4$. Fig. 2(b) depicts the crystal structure of $Mg_{1-x}Co_xMoO_4$. $MgMoO_4$ is comprised by MgO_6 octahedron with the layered arrangement. MgO_6 octahedral layers are connected by MoO_4 tetrahedron. Every four MgO_6 octahedrons are connected by sharing edges to form a cross-shaped unit. Mg^{2+} has two types of coordination environment. In the monoclinic structure, two different types of Mg^{2+} have similar Mg-O distances and coordination numbers [22,

[23]. As Co^{2+} is doped, Co^{2+} occupies the MgO_6 octahedron site.

Fig. 3 exhibits the SEM micrographs of $Mg_{1-x}Co_xMoO_4$ ceramics. $Mg_{1-x}Co_xMoO_4$ ceramic has a dense microstructure with few pores when it is sintered at 975 ° C. The average grain size of ceramics is approximately 10 μm, which is larger than the grain size of $MgMoO_4$ ceramics (approximately 2 μm). When the Co substitution content is 1 mol%, the grain size significantly varies. The grain sizes of ceramics are almost unchanged with Co substitution contents of 5-15 mol%.

Fig. 4 illustrates the relative densities of $Mg_{1-x}Co_xMoO_4$ (x = 0.01–0.15) ceramics sintered from 900 °C to 1000 °C. The relative densities increase with increasing sintering temperature. During the sintering process, grains grow normally in a suitable temperature range. At the same sintering temperature, the relative densities increase from 94 % to 95.5 % with increasing Co content. Therefore, the Co substitution benefits the densification of $MgMoO_4$ ceramics.

Fig. 5 (a) exhibits the change in dielectric constant ε_r of $Mg_{1-x}Co_xMoO_4$ (x = 0.01–0.15) ceramics sintered from 900 °C to 1000 °C. In general, ε_r increases with increasing sintering temperature. In addition, ε_r increases with increasing Co content. As is known, dielectric polarizabilities have obvious effects on the dielectric constant. The theoretical polarizability of materials is calculated by formula (2), where $\alpha(Mg^{2+})$ is 1.33, $\alpha(Co^{2+})$ is 1.65, $\alpha(Mo^{6+})$ is 3.28, and $\alpha(O^{2-})$ is 2.01. The difference between $\alpha(Mg^{2+})$ and $\alpha(Co^{2+})$ results in the variation of dielectric constant.

$$\alpha_{theo} = \alpha(Mg_{1-x}Co_xMoO_4) = (1-x)\alpha(Mg^{2+}) + x\alpha(Co^{2+}) + \alpha(Mo^{6+}) + 4\alpha(O^{2-}) \quad (2)$$

The dielectric polarizability α_m is obtained by Clausius-Mossotti equation (3).

$$\alpha_m = \frac{V_m(\varepsilon_r-1)}{Zb(\varepsilon_r+2)} \quad (3)$$

V_m, b, Z, and ε_r are the unit cell volume, a constant ($4\pi/3$), number of molecules in a single unit cell (Z = 8 in our system), and dielectric constant of the samples, respectively. Clausius-Mossotti equation indicates that ε_r is determined by α_m/V_m. As Fig. 5 (b) shows, α_m/V_m linearly increases with increasing Co content. The ε_r values of $Mg_{1-x}Co_xMoO_4$ display a similar trend with α_m/V_m. ε_r increases from 6.94 to 7.26

when the Co content increases from 1 to 15 mol%. In addition, ε_r exhibits a similar trend with the relative densities. Therefore, the dielectric polarizability and relative densities are the main factors that control ε_r of ceramics.

Fig. 6 shows the τ_f values of $Mg_{1-x}Co_xMoO_4$ ceramics sintered at 975 °C. The τ_f values increase from -63 to -88 ppm/°C when the Co content increases. Compared with pure $MgMoO_4$ ceramics (-70 ppm/°C), τ_f does not improve as expected.

T The variations in $Q\times f$ of $Mg_{1-x}Co_xMoO_4$ (x = 0.01–0.15) ceramics at different sintering temperatures for 3 h are shown in Fig. 7. The optimized sintering temperature is 975 °C for the highest $Q\times f$ value (59247 GHz). Compared with $MgMoO_4$ ceramics (~49149 GHz), the incorporation of Co obviously improves $Q\times f$ values of ceramics. When the Co content changes from 0.01 to 0.05, $Q\times f$ increases from 53459 to 59247 GHz. $Q\times f$ is enhanced by approximately 10000 GHz compared to pure $MgMoO_4$ ceramics. When the Co content continues to increase to 0.15, $Q\times f$ decrease to 50749 GHz. Therefore, the Co incorporation is beneficial for higher $Q\times f$.

$Q\times f$ values are influenced by many factors, including the density, abnormal grain growth, packing fraction, and secondary phase. The XRD and sintering performance analysis show that single-phase $Mg_{1-x}Co_xMoO_4$ ceramics have high densities. Higher density always benefits $Q\times f$ values, so $Q\times f$ increases with Co content increasing to 0.05. However, when the Co content is higher than 0.05, $Q\times f$ reduces. The relative density effect cannot explain the decrease in $Q\times f$ values. It can be expected that intrinsic factors such as polyhedral distortion, order–disorder arrangement of ions and packing fraction are the main influencing factors. $Q\times f$ values are associated with the packing fraction, which is defined in formula (4). V_m, V_p, and Z are the unit cell volume, sum of all packed ion volumes, and number of molecules in a single unit cell (Z = 8), respectively. As Fig. 8 shows, the increased Co content causes a decrease in packing fraction. Thus, the intrinsic loss increases, and $Q\times f$ decreases when the Co content is over 5 mol%.

$$Packing\ Fraction = \frac{Z\times V_p}{V_m} \quad (4)$$

The raw material in the experiment is CoO. However, during the sintering

process, Co^{2+} in $Mg_{1-x}Co_xMoO_4$ ceramics will partially change into Co^{3+}. As Fig. 9 shows, the chemical states of Co ions in $Mg_{1-x}Co_xMoO_4$ ceramics are studied by XPS. The binding energy for Co^{2+} $2p_{1/2}$, Co^{2+} $2p_{3/2}$, Co^{3+} $2p_{1/2}$ and Co^{3+} $2p_{3/2}$ is 796 eV, 780 eV, 797.5 eV and 783 eV, respectively[24-26]. The XPS indicates that the oxidation states of Co element in $Mg_{1-x}Co_xMoO_4$ ceramics are Co^{2+} and Co^{3+}. Co^{3+} doping causes ionic compensation which produces an increase disorder. The disorder distribution of ions in A-sites will contribute to an increase in dielectric loss.

Raman spectroscopy is effective in characterizing order – disorder structures. In group theory [27-29], there are 69 modes (19Ag + 14Au + 17Bg +19Bu). Among these modes, there are 36 internal and lattice modes of the MoO_4 tetrahedron (11Ag + 8Au + 7Bg + 10Bu) [30, 31], including symmetric stretching modes ν_1 (2Ag+ 1Au + 1Bu), anti-symmetric stretching modes ν_3 (3Ag + 2Au + 3Bg + 4Bu), symmetric bending modes ν_2 (3Ag + 3Au + 1Bg + 1Bu) and anti-symmetric bending modes ν_4 (3Ag + 2Au + 3Bg + 4Bu). The lattice modes include translations of Mg^{2+} (3Ag + 2Au + 3Bg + 4Bu) and $MoO4^{2-}$ ions (3Ag + 2Au + 3Bg + 4Bg) and vibrations of MoO_4^{2-} ions (2Ag + 3Au + 4Bg + 3Bu). As Fig. 10 (a) shows, the peaks at low frequencies represent lattice modes. The peaks at medium frequencies refer to the mix of lattice modes and bending modes. The Mo-O bending modes are located at medium frequencies (ν_2 and ν_4). The peaks at high frequencies (ν_1 and ν_3) represent the Mo-O stretching modes. The Raman peaks become weaker and broader when the Co content exceeds 5 mol%. The appearance of weaker and broader peaks implies that more lattice Raman modes are appearing, and the MoO_4 tetrahedron is disordered [14].

The FWHM of Raman spectra is always related to the order of the crystal structure. The lower FWHM implies longer lifetime of phonon and less interaction with other phonons, which consumes less energy and results in lower intrinsic dielectric loss or higher $Q \times f$ value [32, 33]. As Figs. 10 (c)–(e) show, in general, the FWHM values of lattice Raman modes and Mo-O stretching modes have an uptrend with increasing Co content, especially when the Co content exceeds 5 mol%. This phenomenon is due to the disorder arrangement of A-site ions, which results in the Raman spectra broadening and increasing FWHM values. In particular, when the Co

content exceeds 5 mol%, the FWHM values rapidly increases. It is reported that the disorder distribution of ions can break the periodic arrangement of charges, which changes the ionic polarizabilities and increases dielectric loss[16]. The changes of ionic polarizabilities are also the main factor of increasing ε_r. As Fig. 10 (b) shows, when the Co content exceeds 5 mol%, $Q\times f$ sharply reduces. Increasing dielectric loss is due to the disorder distribution of ions when Co is excessively doped. Co doping can benefit the densification of ceramics and increase $Q\times f$ values, but excessive doping will result in the disorder distribution of ions.

Fig. 11 displays the FT-IR spectra of $Mg_{1-x}Co_xMoO_4$ ceramics sintered at 975 °C. The infrared peaks at approximately 740 cm^{-1}, 827 cm^{-1}, 892 cm^{-1}, 938 $cm^{-1}$and 998 cm^{-1} represent the Mo-O stretching vibrations of MoO_4 tetrahedron[34]. The infrared peaks at approximately 430 cm^{-1} represent the bending vibration in MoO_4 tetrahedron. These infrared peaks belong to the internal modes. According to the literature [35], the position and intensity of peaks of internal modes are affected by distorted MoO_4 tetrahedron. Compared with the $MgMoO_4$ FT-IR spectra, the position of the peaks does not shift, and the intensity of the peaks of internal modes slightly weakens with increasing Co content. The result indicates that internal loss, which is due to the distorted MoO_4 tetrahedron, barely contributes to the microwave dielectric properties. Thus, the internal loss of $Mg_{1-x}Co_xMoO_4$ ceramics is mainly generated by the packing fraction, and the extrinsic loss is mainly generated by the disorder distribution of ions in A sites.

4 Conclusions

$Mg_{1-x}Co_xMoO_4$ ceramics were successfully prepared by the traditional solid-state method. The structural analysis indicates that the $Mg_{1-x}Co_xMoO_4$ solid solution has a monoclinic wolframite structure at x from 0.01 to 0.15. The ceramics sintered at 900-1000 °C had dense microstructures. The best sintering temperature is 975 °C. Co substitution benefits the densification of $MgMoO_4$ ceramics and improves the $Q\times f$ values of $MgMoO_4$ ceramics. The addition of Co increases the dielectric constant of $Mg_{1-x}Co_xMoO_4$ ceramics. Dielectric polarizability and relative densities are the main factors that govern the ε_r values of the ceramics. There is no significant improvement

for τ_f when the Co content increases. For $Q\times f$, $Mg_{1-x}Co_xMoO_4$ (x = 0.01–0.15) ceramics have higher $Q\times f$ values than $MgMoO_4$ ceramics. The maximal $Q\times f$ values occur at 5 mol% Co^{2+} content. Increased Co content causes a decrease in packing fraction and an increase in intrinsic losses. $Mg_{0.95}Co_{0.05}MoO_4$ ceramic exhibits an optimal microwave dielectric property: ε_r = 7, $Q\times f$ = 59247 GHz, τ_f = -68 ppm/°C. The Raman spectra show that the degree of disorder distribution increases, especially when the Co content exceeds 5 mol%, which worsens their $Q\times f$ values. The FT-IR spectra indicate that the distorted MoO_4 tetrahedron barely contributes to the microwave dielectric properties of ceramics. Therefore, the disorder distribution of ions in A-sites and decreased packing fraction are the main factors that affect the microwave dielectric properties.

Acknowledgements

This work was supported by the Opening Project of the State Key Laboratory of Advanced Materials and Electronic Components (No. FH2015RDZ001), Priority Academic Program Development of Jiangsu Higher Education Institutions (PAPD), the Top-notch Academic Programs Project of Jiangsu Higher Education Institutions (TAPP, PPZY2015B128) and the Jiangsu Collaborative Innovation Center for Advanced Inorganic Function Composites.

References

[1] M.T. Sebastian, Dielectric materials for wireless communication, (2008).

[2] I.M. Reaney, D. Iddles, Microwave dielectric ceramics for resonators and filters in mobile phone networks, J. Am. Ceram. Soc. 89 (2006) 2063-2072.

[3] E.S. Kim, B.S. Chun, R. Freer, R.J. Cernik, Effects of packing fraction and bond valence on microwave dielectric properties of $A^{2+}B^{6+}O_4$ (A^{2+}: Ca, Pb, Ba; B^{6+}: Mo, W) ceramics, J. Eur. Ceram. Soc. 30 (2010) 1731-1736.

[4] J. Guo, D. Zhou, L. Wang, H. Wang, T. Shao, Z.M. Qi, X. Yao, Infrared spectra, Raman spectra, microwave dielectric properties and simulation for effective permittivity of temperature stable ceramics $AMoO_4$-TiO_2 (A = Ca, Sr), Dalton Trans. 42 (2013) 1483-1491.

[5] X.C. Lu, W.J. Bian, Y.Y. Li, H.K. Zhu, Z.X. Fu, Q.T. Zhang, Influence of inverse spinel structured $CuGa_2O_4$ on microwave dielectric properties of normal spinel $ZnGa_2O_4$ ceramics, J. Am.

Ceram. Soc. 101 (2018) 1646-1654.

[6] B. Quan, W.H. Shi, S.J.H. Ong, X.C. Lu, P.L.Y. Wang, G.B. Ji, Y.F. Guo, L.R. Zheng, Z.C.J. Xu, Defect engineering in two common types of dielectric materials for electromagnetic absorption applications, Adv. Funct. Mater. 29 (2019).

[7] M.T. Sebastian, H. Jantunen, Low loss dielectric materials for LTCC applications: a review, Int. Mater. Rev. 53 (2008) 57-90.

[8] G.K. Choi, J.R. Kim, S.H. Yoon, K.S. Hong, Microwave dielectric properties of scheelite (A = Ca, Sr, Ba) and wolframite (A = Mg, Zn, Mn) $AMoO_4$ compounds, J. Eur. Ceram. Soc. 27 (2007) 3063-3067.

[9] L.J. Tang, J.W. Zhai, H.J. Zhang, X. Yao, Microwave dielectric properties of tunable $Ba_{0.5}Sr_{0.5}TiO_3$ and scheelite $AMoO_4$ (A = Ba, Sr) composite ceramics, J. Alloy. Compd. 551 (2013) 556-561.

[10] J. Guo, C.A. Randall, G.Q. Zhang, D. Zhou, Y.Y. Chen, H. Wang, Synthesis, structure, and characterization of new low-firing microwave dielectric ceramics: $(Ca_{1-3x}Bi_{2x}\Phi_x)MoO_4$, J. Mater. Chem. C 2 (2014) 7364–7372.

[11] E.S. Kim, C.J. Jeon, P.G. Clem, Effects of crystal structure on the microwave dielectric properties of ABO_4 (A = Ni, Mg, Zn and B = Mo, W) ceramics, J. Am. Ceram. Soc. 95 (2012) 2934-2938.

[12] L.X. Pang, D. Zhou, W.G. Liu, Low-temperature sintering and microwave dielectric properties of $CaMoO_4$-based temperature stable LTCC material, J. Am. Ceram. Soc. 97 (2014) 2032-2034.

[13] J. Guo, D. Zhou, H. Wang, X. Yao, Microwave dielectric properties of $(1-x)ZnMoO_4$-$xTiO_2$ composite ceramics, J. Alloy. Compd. 509 (2011) 5863-5865.

[14] J. Guo, D. Zhou, Y. Li, T. Shao, Z.M. Qi, B.B. Jin, H. Wang, Structure-property relationships of novel microwave dielectric ceramics with low sintering temperatures: $(Na_{0.5x}Bi_{0.5x}Ca_{1-x})MoO_4$, Dalton Trans. 43 (2014) 11888-11896.

[15] H.H. Xi, D. Zhou, H.D. Xie, B. He, Q.P. Wang, Raman spectra, infrared spectra, and microwave dielectric properties of low-temperature firing $(Li_{0.5}Ln_{0.5})_{1-x}Ca_xMoO_4$ (Ln = Sm and Nd) solid solution ceramics with scheelite structure, J. Am. Ceram. Soc. 98 (2015) 587-593.

[16] H. Tamura, Microwave dielectric losses caused by lattice defects, J. Eur. Ceram. Soc. 26

(2006) 1775-1780.

[17] Z.F. Wang, B.Y. Huang, L.X. Wang, Z.X. Fu, Q.T Zhang, Low loss $(Ba_{1-x}Sr_x)(Co_{1/3}Nb_{2/3})O_3$ solid solution: phase evolution, microstructure and microwave dielectric properties, J. Mater. Sci. Mater. Electron. 26 (2015) 4273-4279.

[18] K. Wakino, M. Murata, H. Tamura, Far infrared reflection spectra of $Ba(Zn,Ta)O_3$-$BaZrO_3$ dielectric resonator material, J. Am. Ceram. Soc. 69 (1986) 34-37.

[19] M.H. Chen, D.B. Tanner, J.C. Nino, Infrared study of the phonon modes in bismuth pyrochlores, Phys. Rev. B 72 (2005).

[20] L.C. Robertson, M. Gaudon, S. Jobic, P. Deniard, A. Demourguess, Investigation of the first-order phase transition in the $Co_{1-x}Mg_xMoO_4$ solid solution and discussion of the associated thermochromic behavior, Inorg. Chem. 50 (2011) 2878-2884.

[21] W.J. Bian, X.C. Lu, Y.Y. Li, C.F. Min, H.K. Zhu, Z.X. Fu, Q.T. Zhang, Influence of Nd doping on microwave dielectric properties of $SrTiO_3$ ceramics, J. Mater. Sci. Mater. Electron. 29 (2018) 2743-2747.

[22] E. Cavalli, A. Belletti, M.G. Brik, Optical spectra and energy levels of the Cr^{3+} ions in MWO_4 (M = Mg, Zn, Cd) and $MgMoO_4$ crystals, J. Phys. Chem. Solids 69 (2008) 29-34.

[23] W.G. Ran, L.L. Wang, M.L. Yang, X.Y. Kong, D. Qu, J.S. Shi, Enhanced energy transfer from Bi^{3+} to Eu^{3+} ions relying on the criss-cross cluster structure in $MgMoO_4$ phosphor, J. Lumin. 192 (2017) 141-147.

[24] Sudha, M. Saxena, K. Balani, T. Maiti, Structure and thermoelectric properties of calcium doped Sr_2TiCoO_6 double perovskites, Mater. Sci. Eng. B-Adv. 244 (2019) 65-71.

[25] H.C. Wang, L. Xiang, W. Wei, J. An, J. He, C.H. Gong, Y.L. Hou, Efficient and Lightweight Electromagnetic Wave Absorber Derived from Metal Organic Framework-Encapsulated Cobalt Nanoparticles, ACS Appl. Mater. Interfaces 9 (2017) 42102-42110.

[26] K.Y. Niu, Y. Xu, H.C. Wang, R. Ye, H.L. Xin, F. Lin, C.X. Tian, Y.W. Lum, K.C. Bustillo, M.M. Doeff, M.T.M. Koper, J. Ager, R. Xu, H.M. Zheng, A spongy nickel-organic CO_2 reduction photocatalyst for nearly 100% selective CO production, Sci. Adv. 3 (2017) e1700921.

[27] S.C. Chang, M.A. Leugers, S.R. Bare, Surface chemistry of magnesium oxide-supported molybdenum oxide: an in situ Raman spectroscopic study, J. Phys. Chem. 96 (1992) 10358-10365.

[28] J.D. Pless, B.B. Bardin, H.S. Kim, D.G. Ko, M.T. Smith, R.R. Hammond, P.C. Stair, K.R.

Poeppelmeier, Catalytic oxidative dehydrogenation of propane over Mg-V/Mo oxides, J. Catal. 223 (2004) 419-431.

[29] T. Thongtem, A. Phuruangrat, S. Thongtem, Characterization of $MMoO_4$ (M=Ba, Sr and Ca) with different morphologies prepared using a cyclic microwave radiation, Mater. Lett. 62 (2008) 454-457.

[30] C. Luz-Lima, J.C. Batista, P.T.C. Freire, G.P. de Sousa, F.E.P. dos Santos, J. Mendes Filho, B.C. Viana, G.D. Saraiva, Temperature-dependent Raman spectroscopy studies of phase transformations in the K_2WO_4 and the $MgMoO_4$ crystals, Vib. Spectrosc. 65 (2013) 58-65.

[31] M.N. Coelho, P.T.C. Freire, M. Maczka, C. Luz-Lima, G.D. Saraiva, W. Paraguassu, A.G. Souza Filho, P.S. Pizani, High-pressure Raman scattering of $MgMoO_4$, Vib. Spectrosc. 68 (2013) 34-39.

[32] X.C. Lu, W.J. Bian, B. Quan, Z.F. Wang, H.K. Zhu, Q.T. Zhang, Compositional tailoring effect on $ZnGa_2O_4$-TiO_2 ceramics for tunable microwave dielectric properties, J. Alloy. Compd. 792 (2019) 742-749.

[33] X.C. Lu, Z.H. Du, B. Quan, W.J. Bian, H.K. Zhu, Q.T. Zhang, Structural dependence of the microwave dielectric properties of Cr^{3+}-substituted $ZnGa_2O_4$ spinel ceramics: crystal distortion and vibration mode studies, J. Mater. Chem. C 7 (2019) 8261-8268.

[34] F.D. Hardcastle, I.E. Wachs, Determination of Niobium-Oxygen Bond Distances and Bond Orders by Raman Spectroscopy, J. Raman Spectrosc. 21 (1990) 683-691.

[35] P. Yadav, E. Sinha, Structural, photophysical and microwave dielectric properties of alpha-$ZnMoO_4$ phosphor, J. Alloy. Compd. 795 (2019) 446-452.

Figure Captions

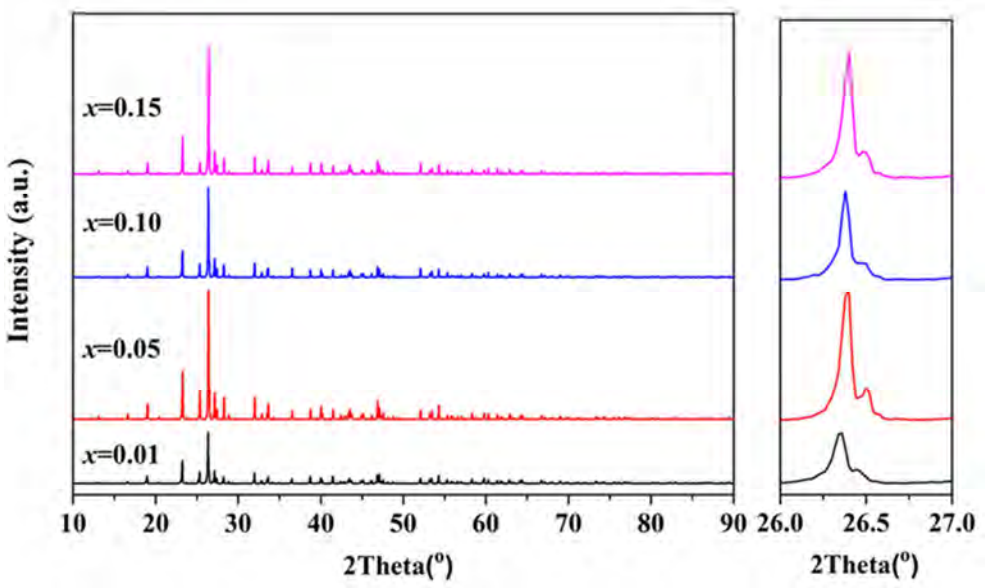

Fig. 1 XRD patterns of $Mg_{1-x}Co_xMoO_4$ ceramics with different *x* values of 10-90° and 26-27° sintered at 975 °C for 3 h.

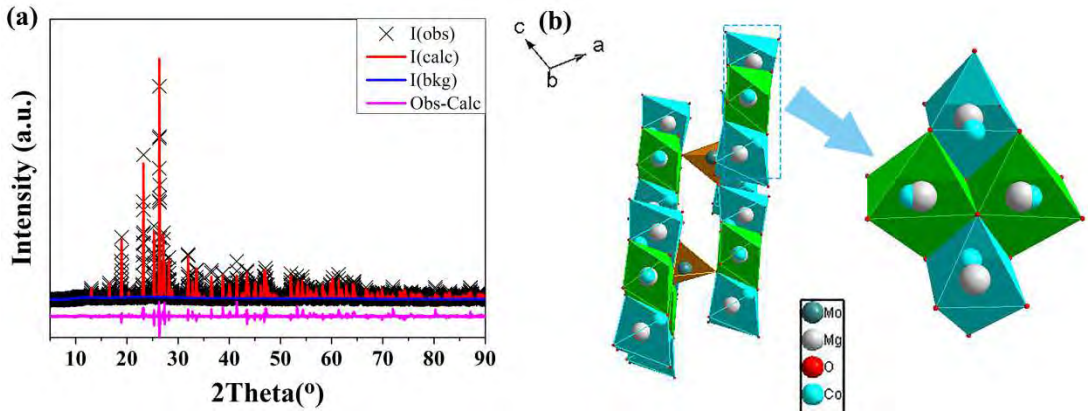

Fig. 2 (a) Rietveld refinements of XRD pattern of $Mg_{0.95}Co_{0.05}MoO_4$ sintered at 975 °C for 3 h. (b) Diagrams of the crystal structure of $Mg_{0.95}Co_{0.05}MoO_4$ sintered at 975 °C for 3 h.

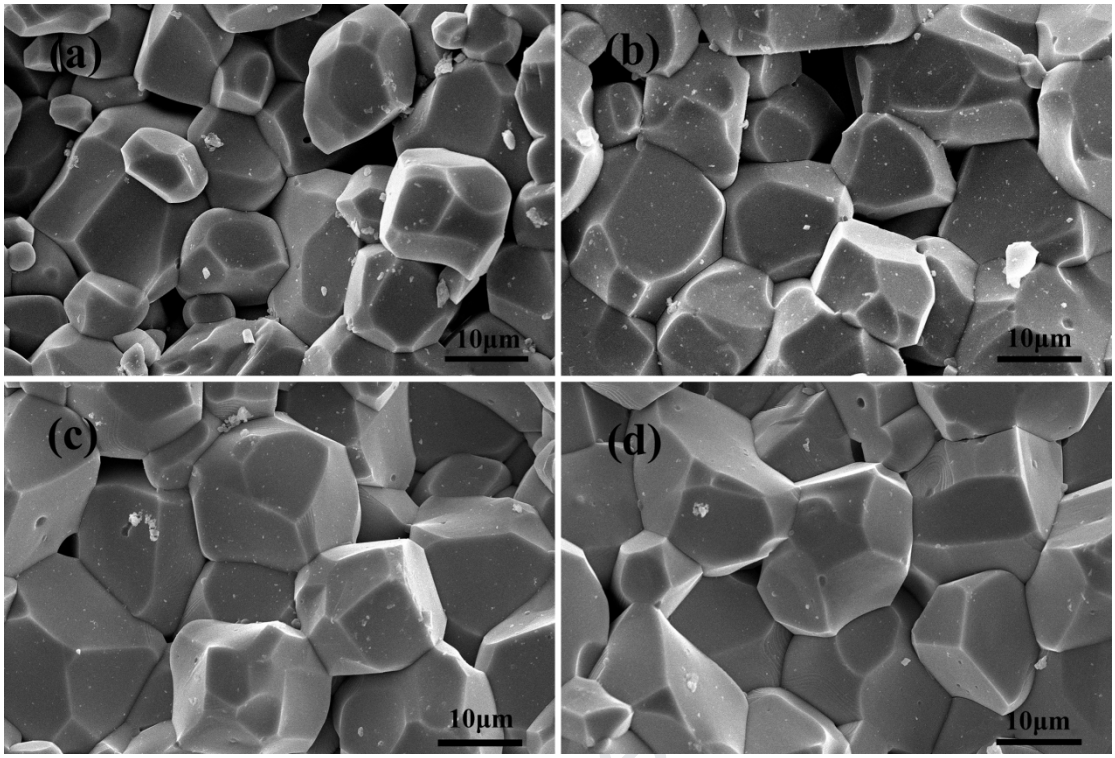

Fig. 3 SEM images of $Mg_{1-x}Co_xMoO_4$ (x = 0.01–0.15) ceramics with (a) x = 0.01, (b) x = 0.05, (c) x = 0.1, (d) x = 0.15, sintered at 975 °C for 3 h.

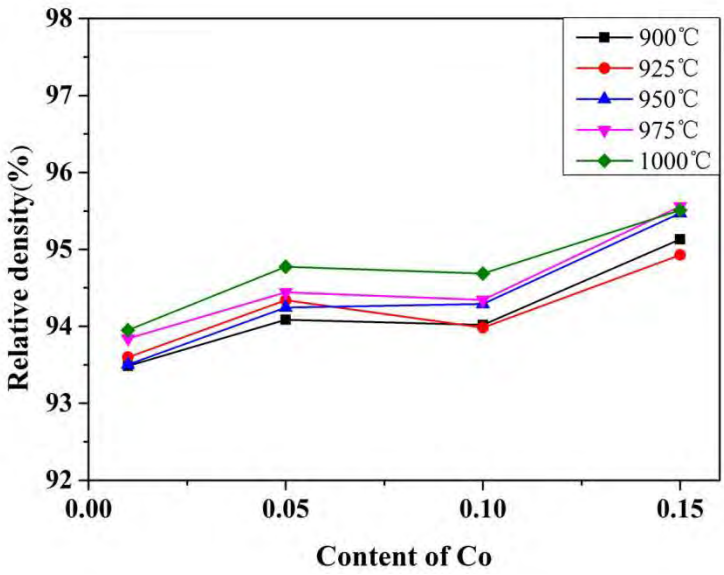

Fig. 4 Relative densities of $Mg_{1-x}Co_xMoO_4$ ceramics with (a) x = 0.01, (b) x = 0.05, (c) x = 0.10, and (d) x = 0.15, sintered at different sintering temperatures.

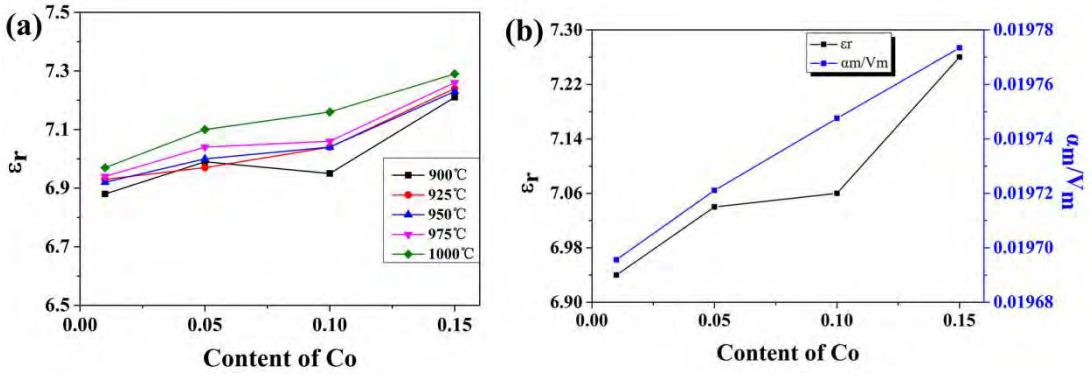

Fig. 5 (a) Variations of the dielectric constant of $Mg_{1-x}Co_xMoO_4$ (x = 0.01–0.15) ceramics at different sintering temperatures. (b) ε_r and α_m/V_m as a function of the Co content.

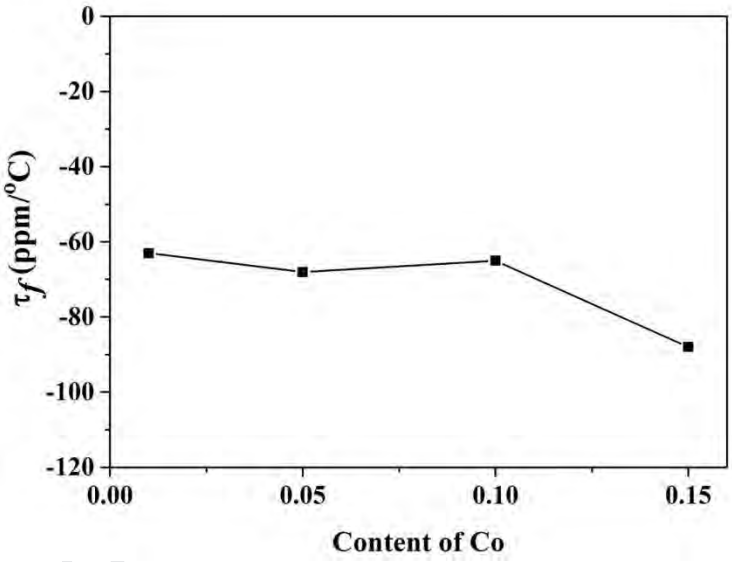

Fig. 6 τ_f values of $Mg_{1-x}Co_xMoO_4$ ceramics with different x values sintered at 975 °C.

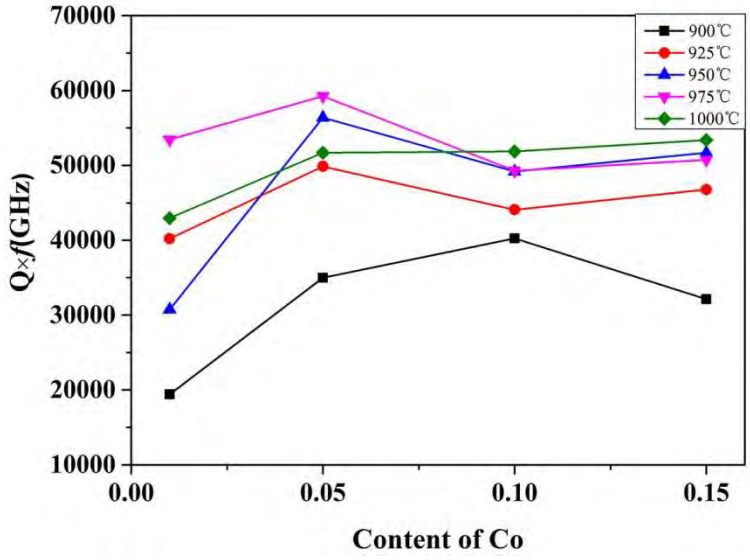

Fig. 7 $Q\times f$ of $Mg_{1-x}Co_xMoO_4$ ceramics with different x, sintered at different temperatures.

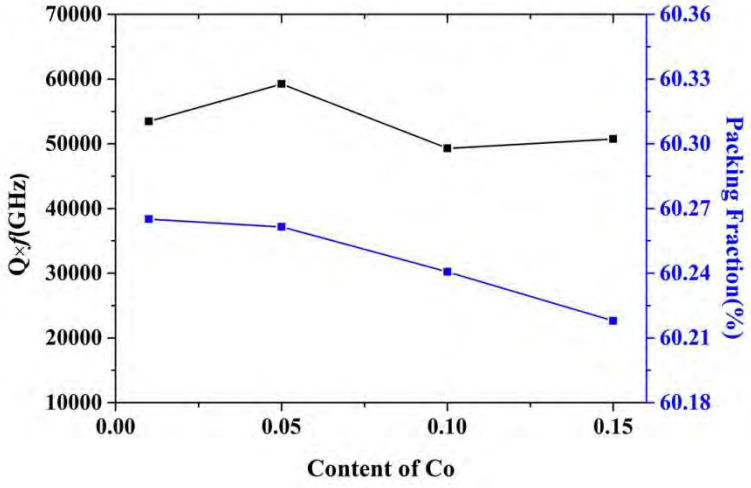

Fig. 8 *Q*×*f* values and packing fraction as a function of Co content, sintered at 975 °C.

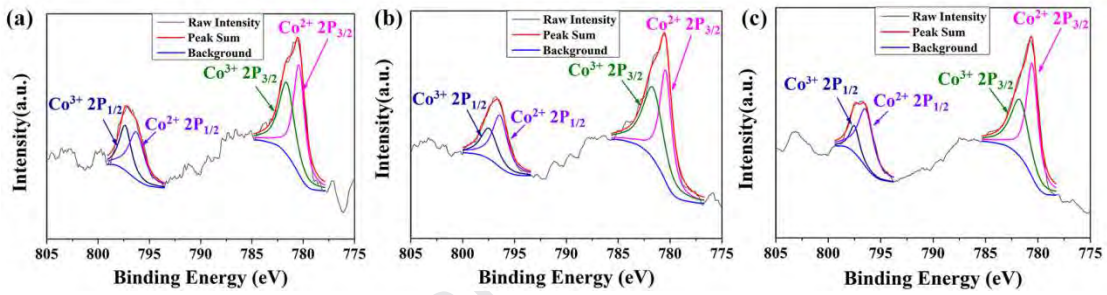

Fig. 9 XPS spectra of Co element (a) x = 0.05; (b) x = 0.10; (c) x = 0.15.

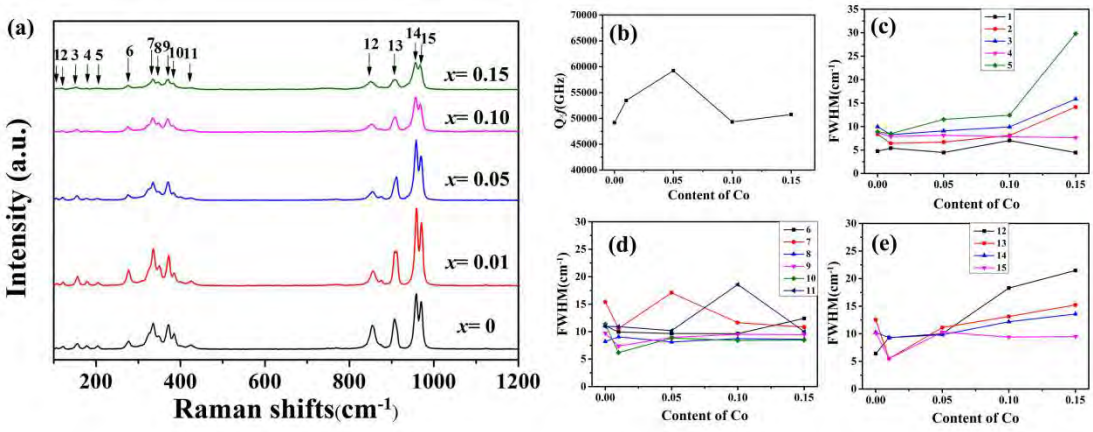

Fig. 10 (a) Raman spectra of $Mg_{1-x}Co_xMoO_4$ ceramics sintered at 975 °C; (b) *Q*×*f* of $Mg_{1-x}Co_xMoO_4$ ceramics sintered at 975 °C; (c) FWHM of peaks 1-5; (d) FWHM of peaks 6-11; (e) FWHM of peaks 12-15.

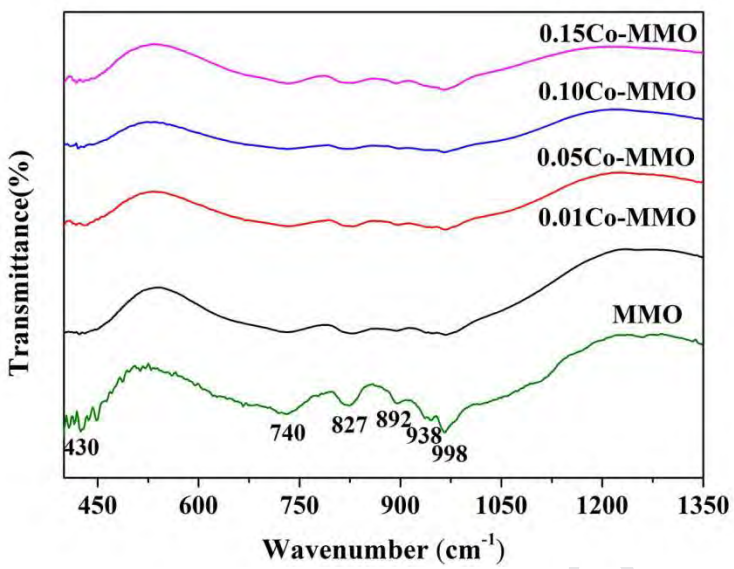

Fig. 11 IR spectra of $Mg_{1-x}Co_xMoO_4$ ceramics sintered at 975 °C.

Tables

Table 1 Refined cell parameters of $Mg_{1-x}Co_xMoO_4$ (x = 0.01–0.15) ceramics sintered at 975 °C for 3 h.

x	a(Å)	b(Å)	c(Å)	α; β; γ (°)	V_m(Å^3)	R_{wp}(%)
0.01	10.2794	9.2921	7.0293	90;106.90;90	642.421	8.22
0.05	10.2779	9.2914	7.0291	90;106.90;90	642.257	7.01
0.10	10.2759	9.2918	7.0299	90;106.91;90	642.206	11.44
0.15	10.2752	9.2920	7.0299	90;106.91;90	642.175	9.87

Conflicts of interest

We declare that we do not have any commercial or associative interest that represents a conflict of interest in connection with the work submitted.